True triaxial testing of geogrid for high speed railways

Z. Yu[1], P. K. Woodward[2], O.Laghrouche[1], D. P. Connolly[2],

[1] *Heriot Watt University, Institute for Infrastructure and Environment, Edinburgh UK*
Email: zy6@hw.ac.uk; O.Laghrouche@hw.ac.uk
[2] *University of Leeds, Institute for High Speed Rail and System Integration. Leeds, UK, LS2 9JT*
Email: D.Connolly@leeds.ac.uk; P.K.Woodward@leeds.ac.uk

Journal: Transport Geotechnics

ABSTRACT:

This work describes a series of novel experimental tests to determine the potential of geogrids to confine granular layers within ballasted railway lines operating at speeds close to critical velocity. This is important because at low train speeds, vertical stresses are dominant, but when approaching critical velocity conditions, dynamic horizontal stress levels are magnified. Therefore the majority of previous geogrid investigations have been performed assuming constant horizontal stress levels, thus making them more relevant for lower speed lines. To investigate settlement under high relative train speeds, ballasted railway track samples were subject to combined vertical-horizontal cyclic loading. Three areas were explored: 1) the performance benefit from placing geogrid at the ballast-subballast interface, 2) the performance benefit from placing geogrid at the subballast-subgrade interface, 3) the effect of subgrade stiffness on geogrid performance at the subballast-subgrade interface. Testing was performed using a unique large-scale true triaxial apparatus which had the ability to vary stress levels in three Cartesian directions. Compared to the control conditions, the geogrid offered a settlement improvement of approximately 35% when placed at the ballast-subballast interface, and 10-15% when placed at the subballast-subgrade interface. Regarding subgrade CBR, it was found that the geogrid offered the greatest performance benefits when the subgrade was soft. Therefore it was concluded that for the ballasted rail structures under test, when subject to elevated levels of horizontal stress, geogrids reduced settlements compared to non-geogrid solutions.

Key words (max 6): True Triaxial Testing Rig; Geogrid Confinement; Ballasted High Speed Railway; Railroad Track Settlement; Cyclic Laboratory Loading; Subballast-Subgrade Geogrid

1 Introduction

Geogrids are commonly used on linear transport infrastructure projects (e.g. roads and railways) to increase the lateral confinement between granular layers, thus improving the longevity of the support structure (Al-Qadi *et al.*, 1994; Hufenus *et al.*, 2006; Kwon, Tutumluer and Konietzky, 2008, Byun *et al.*, 2019). However, on high speed rail lines, vehicles may travel at speeds comparable to the natural wave speed of the underlying soil (i.e. close to critical velocity - Costa *et al.*, (2015); Mezher *et al.*, 2016; Dong *et al.*, 2019), causing the magnification of track deflections ((Kouroussis *et al.*, 2015)). This results in elevated stress levels within both the track and soil, particularly in the horizontal direction (Varandas *et al.*, 2016; Dong *et al.*, 2018). The ability of geogrids to provide similar confinement for rail lines that experience elevated horizontal stresses is currently unclear.

To study the potential performance benefits of geogrid, McDowell *et al.*, (2006) and Ferellec and McDowell, (2012) used the discrete element method to study the influence of ballast shape and geogrid aperture size on ballast–geogrid interlock. They suggested a ratio of geogrid aperture size to particle diameter of 1.4 gave efficient ballast-geogrid interlock. Similarly, Ngo, Indraratna and Rujikiatkamjorn, (2014) and Ngo, Indraratna and Rujikiatkamjorn, (2016) studied the behaviour of coal-fouled, geogrid reinforced ballast, subject to direct shear testing. The contact force distribution and stress orientation was analysed to better understand ballast behaviour during shearing.

As an alternative to numerical modelling, physical models have also been used to investgate geogrid performance. One of the most common apporaches is to perform vertical loading on a test box with rigid boundary conditions, thus simulating a constant confining stress. For example, Raymond(2002) and Raymond and Ismail(2003) used a compression test box (900mm in length, 200mm in width and 325mm in depth), with a transparent glass wall to show that ballasted track experienced reduced settlement when geo-synthetically reinforced. Similarly, using a variety of different sized steel test boxes, McDowell and Stickley(2006), Horníček et al. (2010) and Ruiken et al. (2010) showed that geogrid reduced permanent settlement significantly. Also, Brown, Kwan and Thom (2007) found that geogrid reinforcement benefits were more pronounced for soft subgrade compared to stiff. Further, Liu *et al.*, (2016) used box tests to evaluate the effect of geogrid on ballast particle movement. It was found that the horizontal translation and rotation of ballast were important movement modes under cyclic loading.

A challenge with rigid boundary box testing is that the confining stress is constant, which is not the case for most transport applications. This was explored Lackenby *et al.*, (2007) who showed that confining pressure plays an important role in degradation and deformation resistance. Therefore, Indraratna *et al.*(2006, 2015); Indraratna, Nimbalkar and Christe (2009); Indraratna, Ngo and Rujikiatkamjorn (2012); Indraratna, Hussaini and Vinod (2013) used a bespoke triaxial rig to simulate a range of constant confining stresses. Again it was found that the geogrid generated additional internal confinement at the ballast-subballast interface, thus reducing settlement under a range of constant confining stresses between 5-30kPa. This involved repeating tests multiple times, each with a different (yet constant) confining stress.

However, it has also been shown that in addition to confining stress, the dynamic stresses induced during train passage are also very important (Varandas *et al.*, 2016, (Dyvik and Kaynia, 2018)). Therefore this research builds upon the previously described work, however instead of maintaining a constant confining stress during laboratory testing, it is varied during each load cycle. This is important because when track-ground structures are subject to highly dynamic train loads, horizontal stresses change rapidly. First a true triaxial test rig ('GeoTT') is described which has 6 independent hydraulic rams in three Cartesian directions, thus allowing for the generation of tri-directional cyclic stress patterns. It is then used to make new and novel findings in three areas: 1) the benefits of using geogrid between ballast and subballast in the presence of high horizontal stresses, 2) the benefits of using geogrid between subballast and subgrade in the presence of high horizontal stresses, 3) the effect of varying subgrade CBR on geogrid placed between ballast and subballast, in the presence of high horizontal stresses.

2 Laboratory testing

True triaxial testing of granular railway layers reinforced with geogrid was performed. Three test setups were considered:

- Setup A: A layered ballast-subballast track structure, in the presence and absence of geogrid
- Setup B: A layered subballast-subgrade track structure, in the presence and absence of geogrid
- Setup C: A layered subballast-subgrade track structure, with geogrid and varying subgrade stiffness

2.1 True triaxial testing rig

The true triaxial rig (GeoTT) consisted of 6 independent hydraulic rams, 2 of which were orientated in each Cartesian plane, mounted on a rigid steel frame to apply cyclic load towards the test sample (see Figure 1). The following notation was used for the three Cartesian directions:

- X = direction parallel to the direction of train passage
- Y = direction perpendicular to the direction of train passage
- Z = vertical direction

The test samples were placed inside a bespoke steel cage with dimensions 560 × 560 × 560mm, capable of housing large particle materials such as ballast (Figure 2). The cage had six movable steel walls in each loading direction, thus allowing for volumetric changes of the sample to occur. To prevent the egress of small granular particles via the steel wall-cage clearance, the inner test cage was encased using a thin plastic membrane. More detailed information regarding rig development is presented in (Yu *et al.*, 2019).

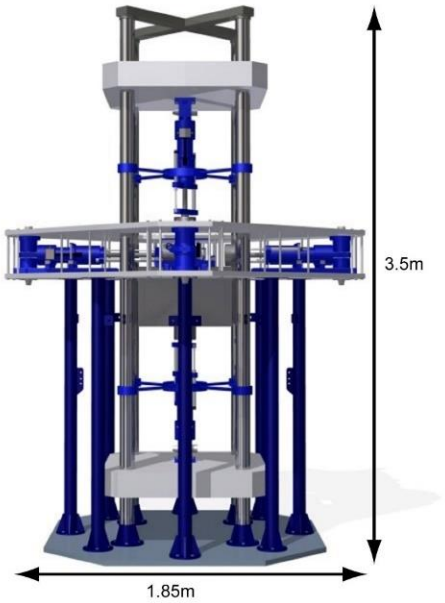

Figure 1: GeoTT Rig design

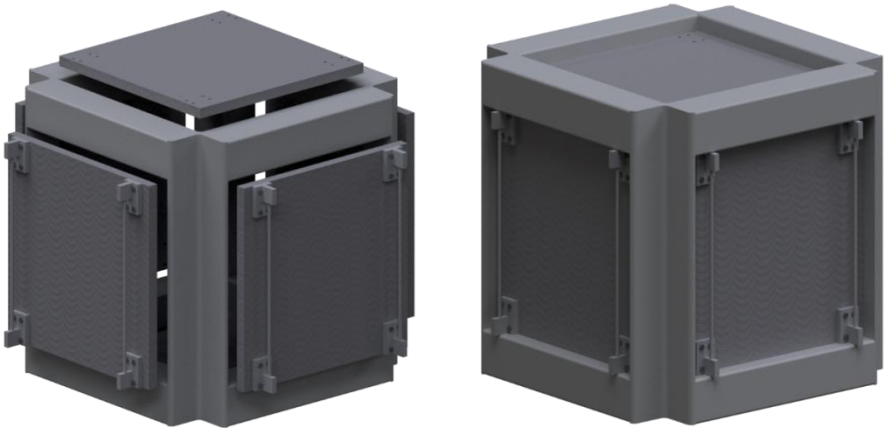

Figure 2. GeoTT testing cage: (left) walls contracted, (right) walls compressed

2.2 Sample preparation

2.2.1 Ballast

The ballast material was a hard angular granite, as commonly used on the rail network in Scotland, UK. The grading of this material (BSI, 2002) is shown in Figure 3. The sample lay within the particle range 20-63mm and was characterised by d_{50} =43mm. There are many ways of quantifying ballast quality (Sadeghi, Emad Motieyan and Ali Zakeri, (2019)), however in this work, the coefficient of uniformity C_u and coefficient of curvature C_c were calculated as 1.36 and 1.009 respectively, indicating the ballast was classified as uniformly graded. Prior to testing the ballast aggregate was washed and dried in accordance with EN 13450-2002 (BSI, 2002) and BS EN 933-1 (BSI, 2005).

Although only particle size distribution tests were used to characterise the ballast, it was sourced from the same Network Rail approved quarry as the ballast used by Kwan, (2006). Therefore the properties were likely to have been similar to those found in other UK ballast research works [e.g. LAA index $\leq$ 20 (BSI, 2010), MDE index $\leq$ 7 (BSI, 2011), ACV $\leq$ 22% (BSI, 1990b), Flakiness index $\leq$ 35 (BSI, 2012), Particle length $\leq$ 4 (BSI, 1996)].

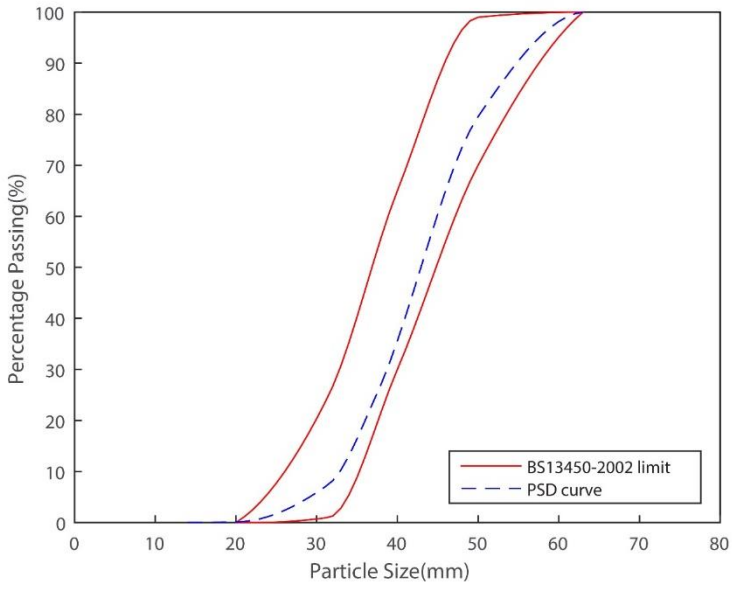

Figure 3. Particle size distribution of ballast

2.2.2 Subballast

The subballast material used in test setups A, B and C complied with Cl 803 (Type 1 sub base) of the UK Specification for Highway works (England, 2016) and also consisted of a hard, angular granite material. The grading curve for this material (BSI, 2002) is shown in Figure 4, giving d_{50} =13mm.

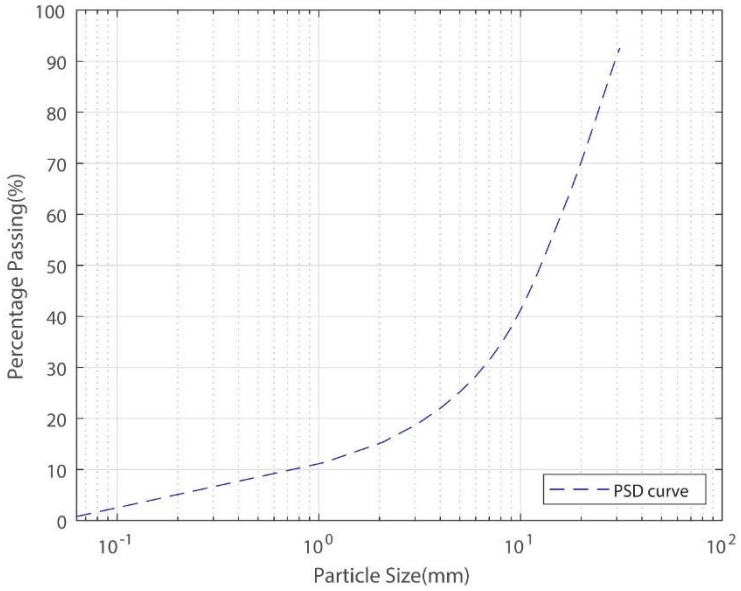

Figure 4. Particle size distribution curve for subballast

2.2.3 Subgrade

The subgrade consisted of 80% kaolin clay (with a high quality medium particle size), and 20% sharp sand with a moisture content of 9.7% ((BSI, 1990a) - Figure 5). Four subgrades with different California bearing ratio (CBR) were tested. To relate CBR to a meaningful qualitative value, Equation (1) (Brown *et al.*, 1987) was used in conjunction with British Standards (2015), as shown in Table 1.

$$C_u = CBR\ value\ \times 20\#(1)$$

Table 1. Description of subgrade with different CBR values

Subgrade CBR Value (%)	Undrained Shear Strength C_u (kPa)	Description
2	40	Soft
3	60	Firm
9	180	Stiff-Very stiff
14	280	Very stiff

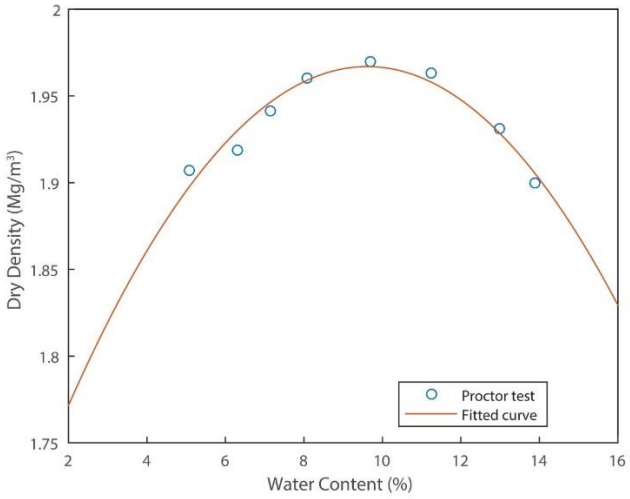

Figure 5. Optimum water content of subgrade

2.2.4 Geogrid

Two types of geogrid were tested. They had different aperture sizes, and chosen to suit the material they were required to provide interlock for:

1. Large aperture: A 190mm aperture size geogrid placed between the ballast and subballast during setup A. It was a triangularly structured, multiaxial geogrid with 60mm long triangular apertures (Figure 6 left). This gave the ratio of the geogrid aperture to ballast particle size as 1.40 (as suggested by McDowell *et al.*, (2006))
2. Small aperture: A 160mm aperture size geogrid: placed between subballast and subgrade during setup B and C. It was a triangularly structured, multiaxial geogrid with 40mm long triangular apertures (Figure 6 right).

The key details of each geogrid are shown in Table 2. For each test, the selvedge edge was orientated parallel to the direction of train passage because this is most commonly used orientation in practise (i.e. the orientation of geogrid when installed on a typical railway track).

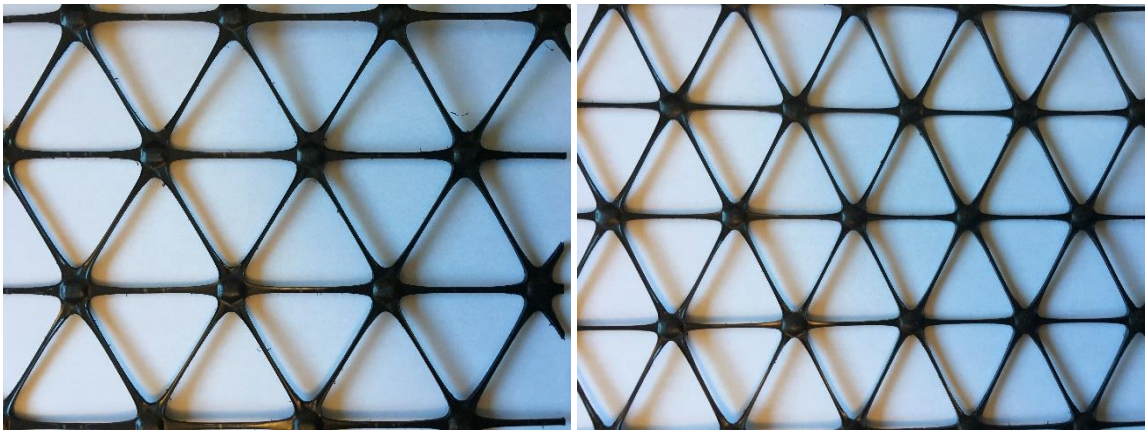

Figure 6. Geogrid arrangement, left: 190mm aperture grid for Setup A; right: 160mm aperture grid for Setups B and C

Table 2. Geogrid specifications

Type	190mm aperture	160mm aperture

Rib pitch (mm)	60	40
Rib shape	Rectangular	Rectangular
Aperture shape	Triangular	Triangular
Test setup	Setup A	Setup B and Setup C

2.3 Loading

Three dimensional finite element modelling was used to generate track-ground stress time histories based upon an 18 tonne axle load travelling at 294km/h over a soft subgrade. The track-soil numerical modelling properties are shown in Table 3. The stress histories were computed at the ballast-subballast interface (for setup A tests) and the subballast-subgrade interface (for setup B tests) (Figure 7). They were then converted to force time histories for use by the GeoTT.

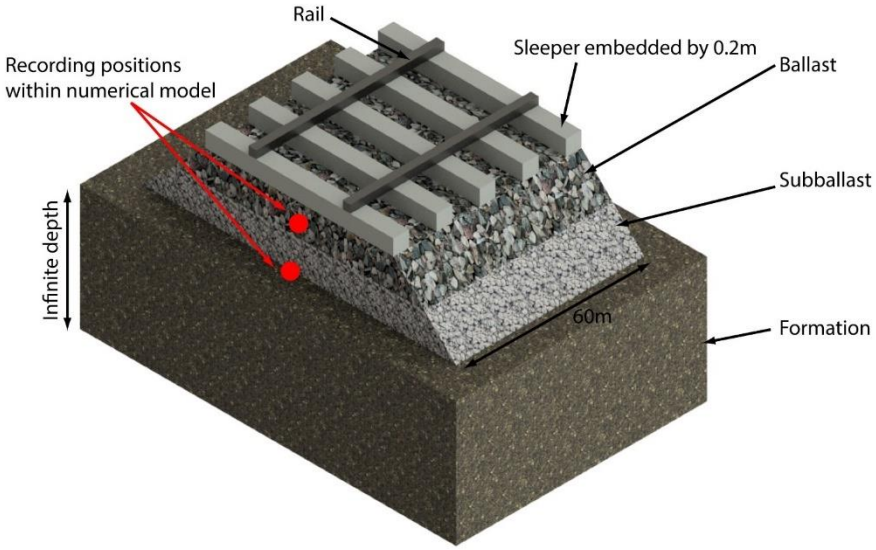

Figure 7. Recording positions of horizontal forces

Table 3. Track numerical modelling properties

	Young's Modulus (MPa)	Poisson' ratio	Density kg/m^3
Rail	210,000	0.3	7800
Sleeper	30,000	0.3	2400
Ballast	150	0.25	1400
Subballast	100	0.3	2200
Formation	46	0.35	2000

2.3.1 Ballast-subballast forces

Using results from the 3D finite element model, the total force on the full-size sleeper was found to be 66kN. Then, converting this to the 0.25m long scaled sleeper, the force on scaled sleeper was 39.6kN. The maximum horizontal nodal stresses from the finite element model sampled at the ballast-subballast interface (red recording position between ballast and subballast layer shown in Figure 7), were 46kPa and 14kPa in parallel and perpendicular direction of train passage respectively. Therefore, multiplying by the cage wall area (0.4m×0.4m), gave the forces required to excite sample Setup A as, 7.36kN and 2.24kN, in parallel and perpendicular direction respectively. Finally, applying

a confining stress of 15kPa consistent with existing literature (Indraratna *et al.*, 2015), the following forces were used:

- Vertical force = 42kN
- Parallel force = 9.76kN
- Perpendicular force = 4.64kN

2.3.2 Subballast-subgrade forces

Using the results from the same 3D finite element model, the mean maximum nodal stresses sampled at the subballast-subgrade interface were 24.23 kPa, 24.10kPa and 6.59kPa in vertical, parallel and perpendicular direction of train passage respectively. Therefore, following a similar ballast-subballast interface calculation, multiplying by the cage wall area (0.4m×0.4m) and accounting for confining stresses gave the forces required for test setups B and C:

- Vertical force = 7.08 kN
- Parallel force = 7.06 kN
- Perpendicular force = 4.25 kN

2.3.3 Time histories

As an example of the force time histories used for GeoTT loading, Figure 8a shows the numerical calculation of the forces required for the ballast-subballast test. Conversely, Figure 8b shows the time histories applied during the laboratory test, which was equivalent to 1 cycle. The numerical result showed a slightly asymmetrical response consistent with high track dynamic response, however for the laboratory test, this was converted into a symmetrical, cyclic response. Also, the frequency of computed result was outside the limits of the GeoTT, meaning it was elongated over a longer time period. Regardless of these modifications, the laboratory forces were judged to be a reasonable approximation of those computed numerically.

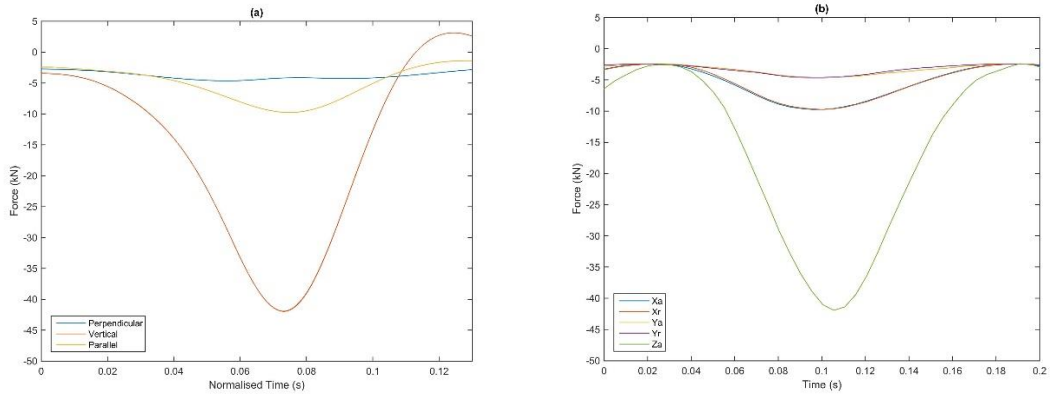

Figure 8. (a) Calculated forces, (b) Idealised cyclic forces used during testing

2.4 Testing programme

Three main test configurations were considered. To have a better understanding of geogrid performance at different locations, geogrid was placed between ballast and subballast (Setup A) and between subballast and subgrade (Setup B). Benchmark tests were undertaken in the absence of geogrid. Finally, to investigate the performance of geogrid in the presence of varying subgrade stiffness, four CBR values were tested. The five rams (Xa, Xr, Ya, Yr, Za) were used to apply cyclic compressive loads between the confining forec and target forces calculated from the numerical work towards ballast samples as shown in Figure 9 and Figure 11. The bottom ram Zr was held the

position throughout all the tests, recording the reaction force. Subscripts 'r' and 'a' are used to differentiate between the 2 different rams in each Cartesian plane. The loading frequency was 6Hz after the target forces reached and a total cycle of 350k was achieved.

2.4.1 Setup A: Ballast-subballast testing

Geogrid (190mm aperture) was installed between the ballast and subballast layers for one of the two tests (Figure 9). A 200mm thick layer of subballast was compacted to a density of 1900 kg/m^3 using a vibrating plate. Once complete, 300mm of ballast was placed on top and compacted to a density of 1400 kg/m^3. A reduced-scale, reinforced concrete sleeper (Figure 10) was embedded into the ballast, which in turn was supported by the subballast layer. The concrete sleeper was cast according to BS 13230-1 (BSI, 2016). The compressive strength of the concrete was C45/55 MPa. The sleeper was trapezoidal in cross section with length 250mm, width 200mm and a height of 150mm. As a control, the test was repeated in the absence of geogrid to permit a direct comparison. The initial forces in all directions were held at 1kN before steadily increasing to the target forces described in section 2.3.1. It should be noted that all six actuators were controlled independently and a limitation of the GeoTT control system meant that each had to be increased sequentially. Therefore the horizontal forces were increased prior to increasing the vertical forces. This meant that during the period between when increasing the horizontal force and reaching the desired vertical force, there was scope for the test sample to expand in the vertical direction. This is evident at the start of the test sample results, where there are localised increases in vertical response immediately prior to the reaching the full loading condition.

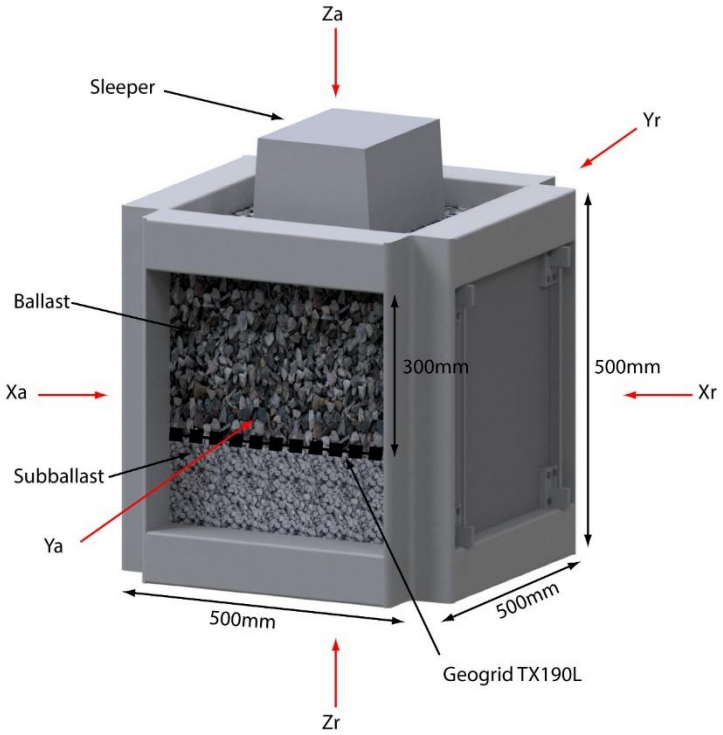

Figure 9. Test Setup A: Geogrid stabilised ballast over sub-ballast (setup A)

Figure 10. Reduced scale sleeper (tie) on top of ballast (Setup A)

2.4.2 Setup B: Subballast-subgrade testing

A subballast layer was supported by a subgrade layer. Geogrid (160mm aperture) was deployed between subballast and subgrade layers for one of the two tests (Figure 11). 'Firm' subgrade (CBR=3%) and 'Stiff-Very stiff' subgrade (CBR=9%) with a thickness of 300mm was compacted in accordance with (BSI, 1990a) using a vibrating plate. The proposed CBR values were measured using a cone penetrometer. Once compaction had been achieved, subballast with height 200mm was placed on top and compacted to a density of 1900 kg/m^3(Figure 12). As a control, the test was repeated in the absence of geogrid. Setup B tests were designed to determine the influence of using geogrid at the location between the subballast and subgrade. The initial forces in all directions were held at 1kN before steadily increasing to the target forces described in section 2.3.2.

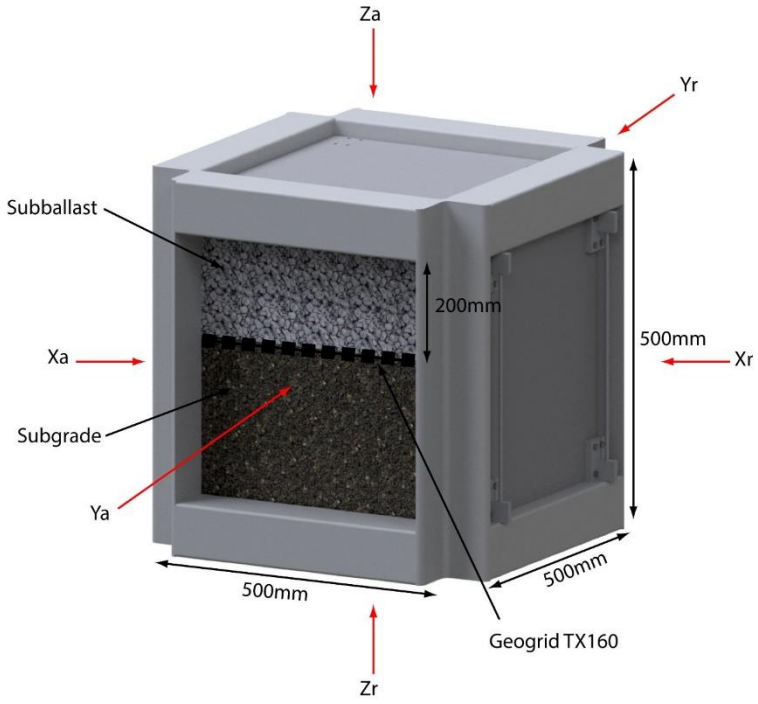

Figure 11. Test Setups B and C: Geogrid stabilised subballast over subgrade

Figure 12. Subballast surface (Setup B)

2.4.3 Setup C: Varying subgrade CBR

The test setup was the same as setup B, however Geogrid (160mm aperture) was deployed between the subballast and subgrade layers for all tests (Figure 11). Four different CBR subgrades were tested: 'Soft' subgrade (CBR=2%), 'Firm' subgrade (CBR=3%), 'Stiff-Very stiff' subgrade (CBR=9%) and 'Very stiff' subgrade (CBR=14%). Each had a thickness of 300mm and was compacted in accordance with (BSI, 1990a) using a vibrating plate. The proposed CBR values were again measured using a cone penetrometer. Once compaction had been achieved, subballast with a height of 200mm was placed on top and compacted to a density of 1900 kg/m3. Setup C tests were designed to determine the benefits of geogrid under varying subgrade CBR, rather than to benchmark the performance of geogrid against the no-geogrid case. The initial forces in all directions were held at 1kN before steadily increasing to the target forces described in section 2.3.2.

3 Results and analysis

3.1 Results interpretation

Vertical, horizontal and overall settlements are defined using Equations (2), (3) and (4):

$$\delta_{vertical} = \delta_Z \#(2)$$

$$\delta_{horizontal} = \delta_X + \delta_Y \#(3)$$

$$\delta_{overall} = \delta_{horizontal} + \delta_{vertical} \#(4)$$

Where:

- δ_X is settlement in the direction of train passage
- δ_Y is settlement perpendicular to train passage
- δ_Z and $\delta_{vertical}$ are the settlements in the vertical direction
- $\delta_{horizontal}$ is settlement in the horizontal direction (combining both parallel and perpendicular directions)
- $\delta_{overall}$ is the overall settlement (combining vertical and horizontal directions)

Also, the average settlement improvement after 350k cycles is computed as shown in Equation (5). Using vertical settlement as an example:

$$\varphi_{vertical} = \frac{\delta_{v1} - \delta_{v2}}{\delta_{v2}} \times 100\% \#(5)$$

Where:

- $\varphi_{vertical}$ is mean vertical settlement improvement
- δ_{v1} is mean vertical settlement during the final 100 data points when the geogrid was present
- δ_{v2} is the mean vertical settlement during the final 100 data points when the geogrid was not present

3.2 Setup A: Geogrid located between ballast and subballast

The settlement response of test setup A in the vertical and horizontal directions after 350k cycles is shown in Figure 13 and Figure 14 respectively. Alternatively, the overall settlement, which combines vertical and horizontal directions, is shown in Figure 15. The definitions of the various settlement metrics are shown in section 3.1, and Table 4 summarises the results. On each figure, there are some small high-frequency oscillations which are artefacts induced when smoothing the data during post-processing.

It was found that the vertical direction exhibited the largest settlement. It was 5.12mm when geogrid was present and 7.81 mm without geogrid, indicating a 34% reduction when using geogrid. Although the horizontal direction experienced lower settlement compared to vertical, the performance benefit was similar for both (35%). The horizontal settlement presented the lateral inward movement of particles in the sample under cyclic confining stress at the point from the numerical model. This suggested that the geogrid placed between ballast and sub-ballast layer helped confine the ballast particles, thus decreasing the lateral settlement/movement of the sample. Similar results have been founded in previous work (e.g. (Brown, Kwan and Thom, (2007) and Indraratna, Ngo and Rujikiatkamjorn, (2013)), however these did not consider the effect of high horizontal stresses. Therefore the new test results confirm that geogrid also offers settlement benefits in the presence of high lateral stresses. It should also be noted that some small and localised settlement recovery was found after 100k cycles. This was attributed to test sample dilation. Similar findings were made for all tests undertaken in this work.

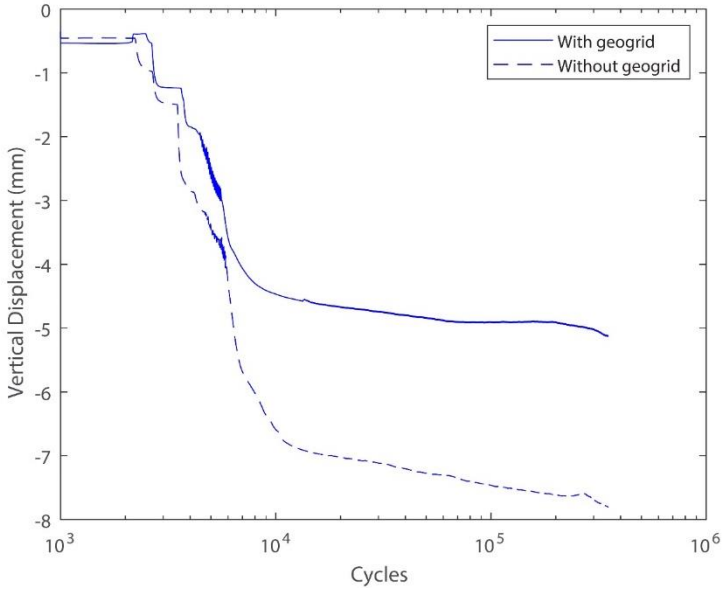

Figure 13. Vertical settlement (Setup A)

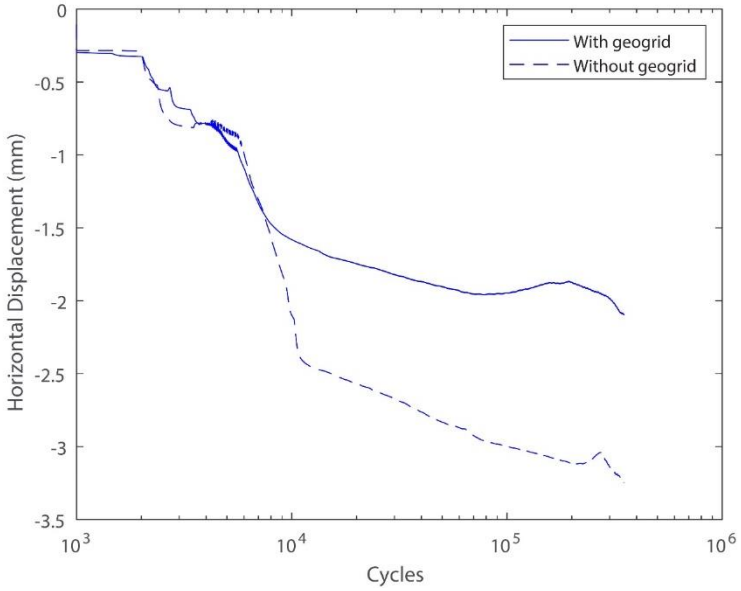

Figure 14. Horizontal settlement (Setup A)

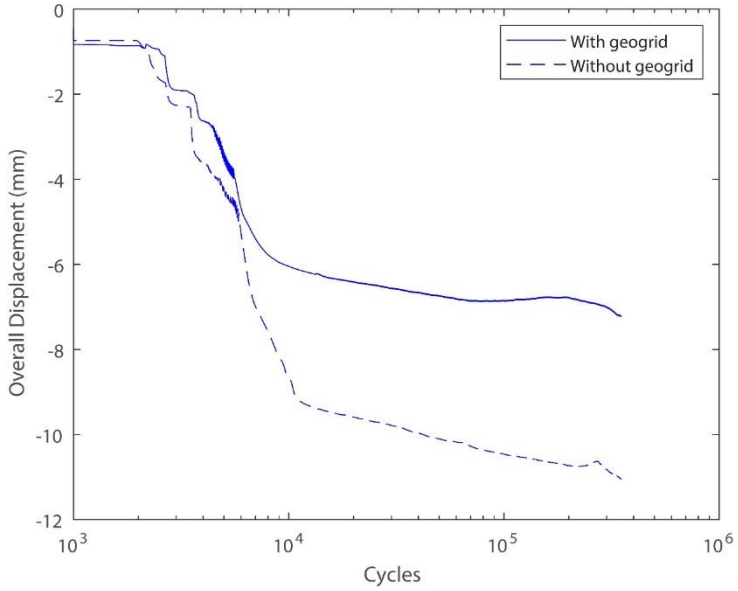

Figure 15. Overall settlement (Setup A)

	Average settlement improvement after 350k cycles Setup A (ballast-subballast)
Horizontal direction	34%
Vertical direction	35%
Overall	35%

Table 4. Settlement comparison of Setup A

3.3 Setup B: Geogrid located between subballast and subgrade

Compared to setup A, setup B was used to investigate geogrid performance when placed at the subballast-subgrade interface. The settlement response of test setup B in the vertical and horizontal directions is shown in Figure 16 and Figure 17 respectively. The overall settlement, which combines vertical and horizontal directions, is shown in Figure 18, while Table 5 summarizes the results.

It is seen that in absence of geogrid, the subgrade with lower values of CBR resulted in a larger settlement in both vertical and horizontal directions. In the vertical direction, it was 1.73mm for the 'firm' subgrade and 1.22mm for the 'Stiff to Very stiff' subgrade. In the horizontal direction it was 1.49mm for the firm subgrade and 1.21mm for the Stiff to 'Very stiff' subgrade. However, after the installation of the geogrid, the vertical settlement in 'firm' and 'Stiff to Very stiff' subgrade consistently decreased by 16% and 13% respectively. Similarly, the horizontal settlement in the 'firm' and 'Stiff to Very stiff' subgrade decreased by 11% for both cases. It should be noted however that a small amount of settlement recovery occurred towards the end of the test. This was attributed to dilation.

The improvements in horizontal settlement were similar for 'firm' and 'stiff-very stiff' subgrade. This suggested that interlock in the horizontal direction improved regardless of the subgrade stiffness. The improvements in overall settlement were 14% and 12% considering 'firm' subgrade and 'stiff-very stiff' subgrade respectively (Table 5). This result is similar to those

from the existing literature which have been performed using constant confining stress. Therefore, for this new situation where there are high lateral stresses, this confirms the benefit of placing geogrid at the sub-ballast-subgrade interface.

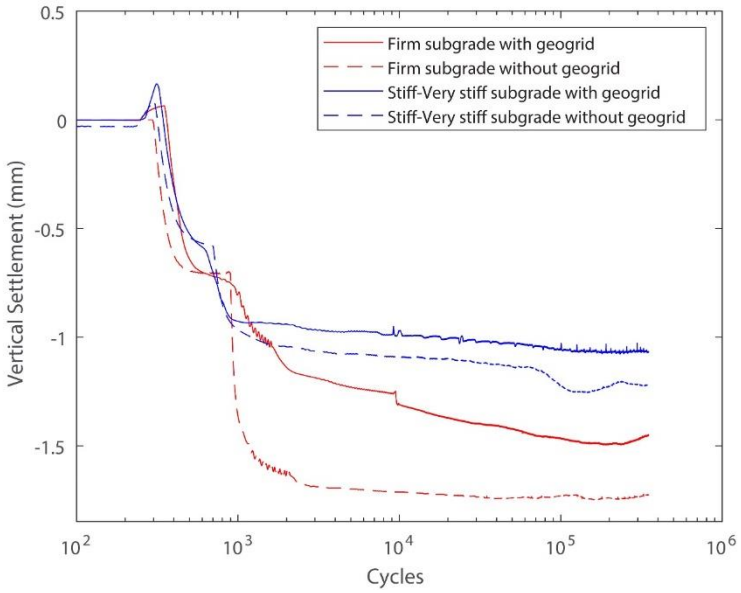

Figure 16. Vertical settlement (Setup B)

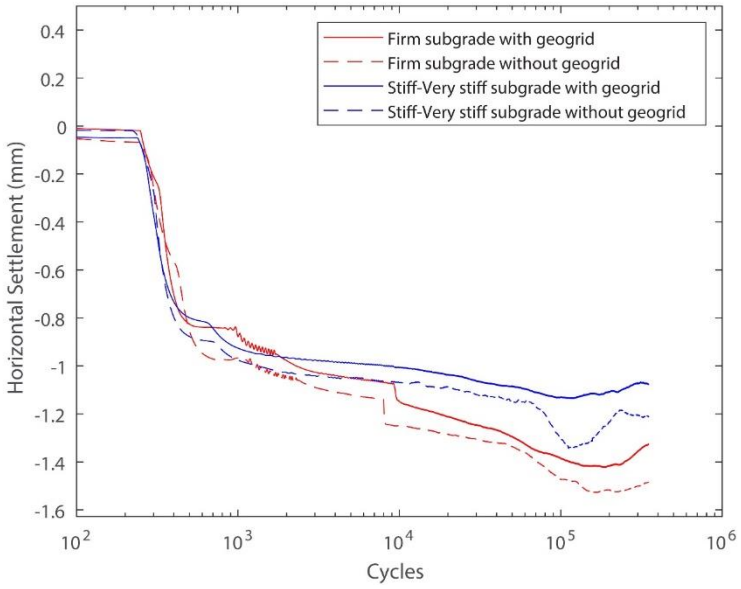

Figure 17. Horizontal settlement (Setup B)

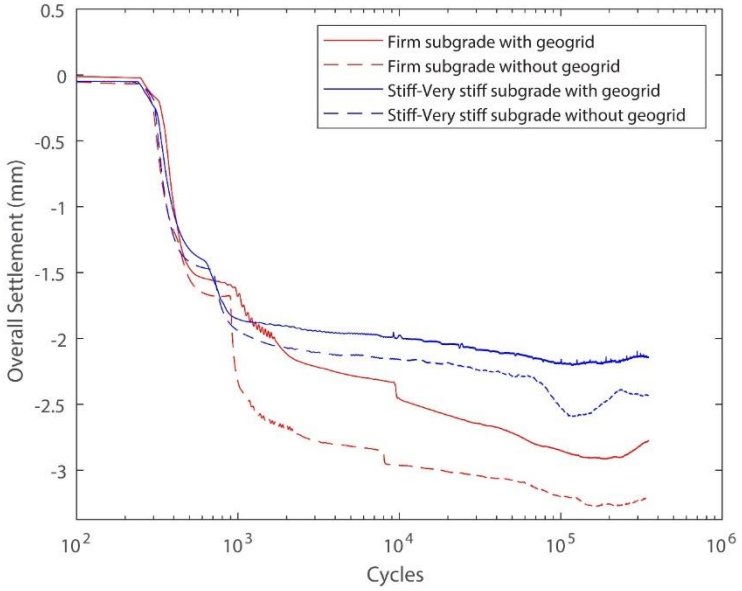

Figure 18. Overall settlement (Setup B)

	Average settlement improvement after 350k cycles (Compared to the results of same subgrade without geogrid)	
	Firm subgrade CBR=3%	**Stiff-Very stiff subgrade CBR=9%**
Vertical direction	16%	13%
Horizontal direction	11%	11%
Overall	14%	12%

Table 5. Settlement comparison (Setup B)

3.4 Setup C: Geogrid performance under varying subgrade stiffness

After setup B showed that the geogrid improved settlement performance when placed at the subballast-subgrade interface, it was tested again using a similar configuration, however in the presence of varying subgrade CBR. The settlement response of test setup C in the vertical direction, combined horizontal directions and overall is shown in Figure 19, Figure 20 and Figure 21 respectively. The total settlements after 350k cycles are shown in Table 6.

Similar to cases A and B, the fastest rate of settlement was found when the total cycles was low, with some elevated localised gradients. In general this was because the granular particles had greatest scope for rearrangement. However it was exacerbated at a small number of discrete cycles because the force was being manually increased towards the target cyclic load, thus introducing some small fluctuations. This finding is magnified in Figure 19-Figure 21 due to using a horizontal-axis log scale, which at low-cycle counts, skews the figure. As the test progressed, settlement continued to increase at 350k cycles, albeit at a slower rate, indicating that the scope for shakedown had been almost fully achieved. In a similar manner to the previous tests however, a small amount of dilation was observed towards the end of the tests.

It was also found that larger settlements occurred in the vertical direction compared to horizontal direction. This was true for all subgrade stiffness's. Also, the stiffer subgrades resulted in lower settlements in all directions. Lower stiffness subgrades were more sensitive to changes in CBR, with small changes resulting in larger reductions to settlement compared to high stiffness subgrade. Compared to the soft subgrade (CBR=2%), the improvements in overall settlement were 18%, 37% and 46% for the firm subgrade (CBR=3%), stiff-very stiff subgrade (CBR=9%), and very stiff subgrade (CBR=14%) respectively. Therefore it can be concluded that when horizontal stresses are high, the benefits of geogrid are higher for soft subgrade compared to very stiff subgrade.

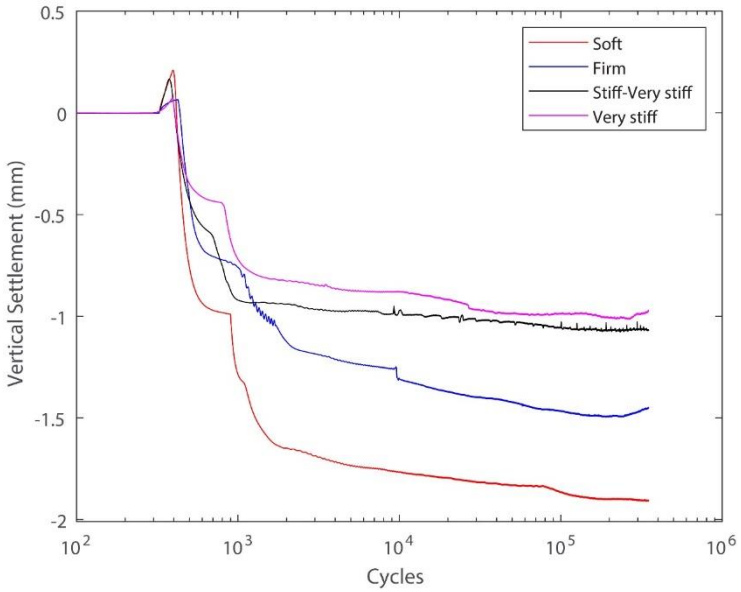

Figure 19. Vertical settlement (Setup C)

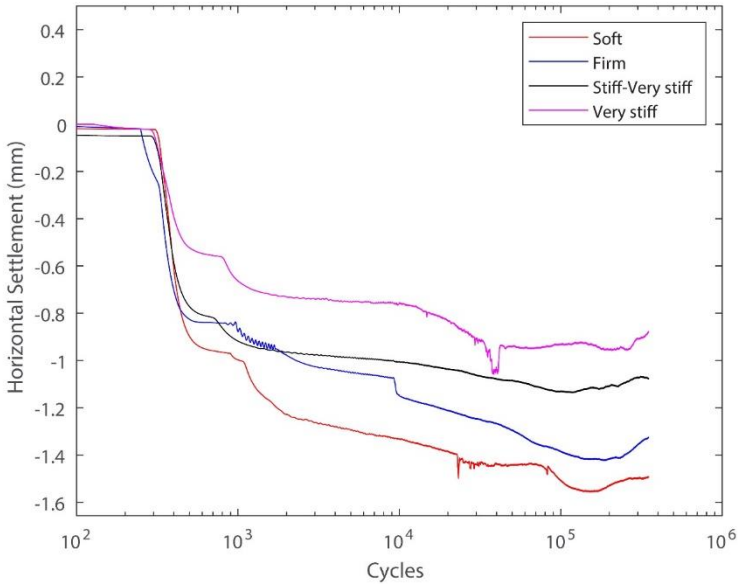

Figure 20. Horizontal settlement (Setup C)

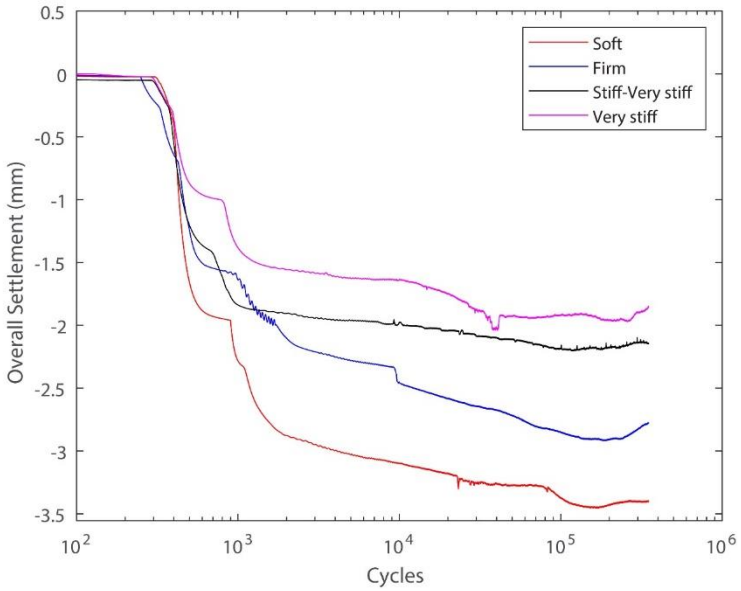

Figure 21. Overall settlement of different subgrades (Setup C)

	Average settlement improvement at 350k cycles (Compared to the results of soft subgrade with CBR=2%)		
	Firm subgrade CBR=3%	**Stiff-Very stiff subgrade CBR=9%**	**Very stiff subgrade CBR=14%**
Vertical direction	24%	44%	49%
Horizontal direction	11%	28%	41%
Overall	18%	37%	46%

Table 6. Settlement comparison of different subgrade stiffness's (Setup C)

4 Conclusions

This report has described a series of experimental tests to determine the potential of geogrids to confine granular layers within ballasted railway lines operating at close to critical velocity. For this speed range, dynamic horizontal stresses are greatly magnified in comparison to vertical stresses, however most research assumes they are constant. Therefore, to investigate this, three main tests were performed under high relative levels of horizontal loading: 1) the performance benefit from placing geogrid at the ballast-subballast interface, 2) the performance benefit from placing geogrid at the subballast-subgrade interface, 3) the effect of subgrade stiffness on geogrid performance at the subballast-subgrade interface. Testing was performed using a unique true triaxial apparatus which had the ability to vary stress levels in the three Cartesian directions. Compared to the control condition, the geogrid offered a settlement improvement of approximately 35% when placed at the ballast-subballast, and 10-15% when placed at the subballast-subgrade interface. Regarding subgrade CBR, it was found that the geogrid offered the greatest performance benefits when the

subgrade was soft. Therefore it was concluded that for the ballasted rail structures under test, when subject to high levels of horizontal stress, geogrids reduced settlements compared to non-geogrid solutions.

Acknowledgements

The authors express their gratitude to Prof David Muir Wood for his significant efforts on the original development of the true triaxial rig. They also thank Heriot-Watt University for the support to modify the original design and adapt it for ballast testing. Also, support from Mr Mike Horton, Tensar and the University of Leeds is gratefully acknowledged.

5 References

Al-Qadi, I. L., Brandon, T. L., Valentine, R. J., Lacina, B. A. and Smith, T. E. (1994) 'Laboratory Evaluation of Geosynthetic-Reinforced Pavement Sections', Transportation Research Record, 1439, pp. 25–31.

Brown, S. F., Kwan, J. and Thom, N. H. (2007) 'Identifying the key parameters that influence geogrid reinforcement of railway ballast', Geotextiles and Geomembranes, 25(6), pp. 326–335.

Brown, S. F., Loach, S. C. and O'Reilly M. P. (1987) Repeated loading of fine grained soils.

BSI (1990a) 'BS 1377-4. Methods of test for soils for civil engineering purposes. Compaction-related tests', British Standards Institution.

BSI (1990b) 'BS 812-111. Testing aggregates. Methods for determination of ten per cent fines value (TFV)', British Standards Institution.

BSI (1996) 'BS EN 933-2. Tests for geometrical properties of aggregates. Determination of particle size distribution. Test sieves, nominal size of apertures', British Standards Institution.

BSI (2002) 'BS EN 13450 Aggregates for railway ballast', British Standards Institution.

BSI (2005) 'BS EN 933-1. Tests for geometrical properties of aggregates Part 1: Determination of Particle Size Distribution - Sieving Method', British Standards Institution, 3(1), pp. 1–7.

BSI (2010) 'BS EN 1097-2. Tests for mechanical and physical properties of aggregates. Methods for the determination of resistance to fragmentation', British Standards Institution.

BSI (2011) 'BS EN 1097-1. Tests for mechanical and physical properties of aggregates. Determination of the resistance to wear (micro-Deval)', British Standards Institution.

BSI (2012) 'BS EN 933-3. Tests for geometrical properties of aggregates. Determination of particle shape. Flakiness index', British Standards Institution.

BSI (2015) 'BS 5930:2015 Code of practice for ground investigations', British Standards Institution.

BSI (2016) ‘BS 13230-1. Railway applications-Track-Concrete sleepers and bearers-Part 1: General requirements’, British Standards Institution.

Byun, Y. H., Tutumluer, E., Feng, B., Kim, J. H. and Wayne, M. H. (2019) ‘Horizontal stiffness evaluation of geogrid-stabilized aggregate using shear wave transducers’, Geotextiles and Geomembranes. Elsevier, 47(2), pp. 177–186.

Costa, P. A., Colaço, A., Calçada, R. and Cardoso, A. S. (2015) ‘Critical speed of railway tracks. Detailed and simplified approaches’, Transportation Geotechnics, 2, pp. 30–46.

Dong, K., Connolly, D. P., Laghrouche, O., Woodward, P. K. and Alves Costa, P. (2018) ‘The stiffening of soft soils on railway lines’, Transportation Geotechnics. Elsevier, 17, pp. 178–191.

Dong, K., Connolly, D. P., Laghrouche, O., Woodward, P. K. and Costa, P. A. (2019) ‘Non-linear Soil Behaviour on High Speed Rail Lines’, Computers and Geotechnics, 112, pp. 302–318.

Dyvik, R. and Kaynia, A. M. (2018) ‘Large-Scale Triaxial Tests on Railway Embankment Material’, in Railroad Ballast Testing and Properties, pp. 173–190.

England, H. (2016) ‘Specification for Highway Works’, Manual of Contract Documents for Highway Works, 1, p. 92.

Ferellec, J.-F. and McDowell, G. R. (2012) ‘Modelling of ballast–geogrid interaction using the discrete-element method’, Geosynthetics International. Thomas Telford Ltd, 19(6), pp. 470–479.

Horníček, L., Tyc, P. and Lidmila, M. (2010) ‘An investigation of the effect of under-ballast reinforcing geogrids in laboratory and operating conditions’, Proceedings of the Institution of Mechanical Engineers, Part F: Journal of Rail and Rapid Transit, 224(4), pp. 269–277.

Hufenus, R., Rueegger, R., Banjac, R., Mayor, P., Springman, S. M. and Brönnimann, R. (2006) ‘Full-scale field tests on geosynthetic reinforced unpaved roads on soft subgrade’, Geotextiles and Geomembranes, 24(1), pp. 21–37.

Indraratna, B., Asce, F., Biabani, M. M. and Nimbalkar, S. (2015) ‘Behavior of Geocell-Reinforced Subballast Subjected to Cyclic Loading in Plane-Strain Condition’, Journal of Geotechnical and Geoenvironmental Engineering, 141(1), p. 04014081.

Indraratna, B., Hussaini, S. K. K. and Vinod, J. S. (2013) ‘The lateral displacement response of geogrid-reinforced ballast under cyclic loading’, Geotextiles and Geomembranes, 39, pp. 20–29.

Indraratna, B., Khabbaz, H., Salim, W. and Christie, D. (2006) ‘Geotechnical properties of ballast and the role of geosynthetics in rail track stabilisation’, Journal of Ground Improvement, 10(3), pp. 91–102.

Indraratna, B., Ngo, N. T. and Rujikiatkamjorn, C. (2012) 'Deformation of coal fouled ballast stabilized with geogrid under cyclic load', Journal of geotechnical and geoenvironmental Engineering, 139(8), pp. 1275–1289.

Indraratna, B., Ngo, N. T. and Rujikiatkamjorn, C. (2013) 'Deformation of Coal Fouled Ballast Stabilized with Geogrid under Cyclic Load', Journal of Geotechnical and Geoenvironmental Engineering, 139(8), pp. 1275–1289.

Indraratna, B., Nimbalkar, S. and Christe, D. (2009) 'The performance of rail track incorporating the effects of ballast breakage , confining pressure and geosynthetic reinforcement', in 8th International Conference on the Bearing Capacity of Roads, Railways, and Airfields, pp. 5–24.

Kouroussis, G., Caucheteur, C., Kinet, D., Alexandrou, G., Verlinden, O. and Moeyaert, V. (2015) 'Review of trackside monitoring solutions: From strain gages to optical fibre sensors', Sensors (Switzerland), 15(8), pp. 20115–20139.

Kwan, C. (2006) Geogrid Reinforcement of Railway Ballast. PhD Thesis, University of Nottingham.

Kwon, J., Tutumluer, E. and Konietzky, H. (2008) 'Aggregate base residual stresses affecting geogrid reinforced flexible pavement response', International Journal of Pavement Engineering, 9(4), pp. 275–285.

Lackenby, J., Indraratna, B., McDowell, G. R. and Christie, D. (2007) 'Effect of confining pressure on ballast degradation and deformation under cyclic triaxial loading', Geotechnique, 57(6), pp. 527–536.

Liu, S., Huang, H., Qiu, T. and Kwon, J. (2016) 'Effect of geogrid on railroad ballast particle movement', Transportation Geotechnics. Elsevier, 9, pp. 110–122.

McDowell, G. R., Konietzky, H., Harireche, O., Brown, S. F. and Thom, N. H. (2006) 'Discrete element modelling of geogrid-reinforced aggregates', Proceedings of the Institution of Civil Engineers - Geotechnical Engineering, 159(1), pp. 35–48.

McDowell, G. and Stickley, P. (2006) 'Performance of geogrid-reinforced ballast', Ground Engineering, 39(1), pp. 26–30.

Mezher, S. B., Connolly, D. P., Woodward, P. K., Laghrouche, O., Pombo, J. and Costa, P. A. (2016) 'Railway critical velocity – Analytical prediction and analysis', Transportation Geotechnics. Elsevier, 6, pp. 84–96.

Ngo, N. T., Indraratna, B. and Rujikiatkamjorn, C. (2014) 'DEM simulation of the behaviour of geogrid stabilised ballast fouled with coal', Computers and Geotechnics. Elsevier, 55, pp. 224–231.

Ngo, N. T., Indraratna, B. and Rujikiatkamjorn, C. (2016) 'Modelling geogrid-reinforced railway ballast using the discrete element method', Transportation Geotechnics. Elsevier, 8, pp. 86–102.

Raymond, G. and Ismail, I. (2003) ‘The effects of geogrid reinforcement on unbound aggregates’, Geotextiles and Geomembranes, 21(6), pp. 355–380.

Raymond, G. P. (2002) ‘Reinforced ballast behaviour subjected to repeated load’, Geotextiles and Geomembranes, 20(1), pp. 39–61.

Ruiken, A., Ziegler, M., Vollmert, L. and Duzic, I. (2010) ‘Recent findings about the confining effect of geogrids from large scale laboratory testing’, in 9th International Conference on Geosynthetics. Brazil, pp. 3–6.

Sadeghi, J., Emad Motieyan, M. and Ali Zakeri, J. (2019) ‘Development of integrated railway ballast quality index’, International Journal of Pavement Engineering. Taylor & Francis, pp. 1–9.

Varandas, J. N., Paixão, A., Fortunato, E. and Hölscher, P. (2016) ‘A Numerical Study on the Stress Changes in the Ballast due to Train Passages 2 The Approach for the Finite Element Analyses’, Procedia Engineering, 143(Ictg), pp. 1169–1176.